Proceedings of the Fifth IIEEJ International Workshop
on Image Electronics and Visual Computing 2017
Da Nang, Vietnam, February 28 - March 3, 2017

COLOR IMAGE DEHAZING BASED ON VISIBLE AND NIR IMAGES FUSION WITH THE TRANSMISSION MAP

Yuhei Kudo[†]
[†]Chuo University

Akira Kubota[††]
[††]Chuo University

ABSTRACT

Outdoor images are degraded by haze. The degraded images can be improved by performing dehazing methods. In this paper, we propose a novel method to dehaze a color image using a near-infrared (NIR) image and a transmission map. NIR images are devoid of haze due to its long wavelength. Our method using the NIR image allows us to recover details and texture in the visible image. Weighting the NIR image with the transmission map, we fuse the NIR and the visible images in the only haze regions. The experimental results demonstrate that our method outperforms the conventional methods.

1. INTRODUCTION

On clear days, the light from distant objects are degraded by haze in outdoor images. Haze is caused by atmospheric particles that scatter the light that enters from the scene to the camera and the atmospheric light. In the captured images, detail of textures is lost.

Dehazing methods have been investigated in recent years. He et al. proposed a dehazing method based on a single haze image[1]. This approach estimates the atmospheric light and the transmission using dark channel prior, and then reconstructs a haze-free image based on the haze image model. However, it is difficult for this method to recover details and texture if the input image loses them.

In contrast, there is another approach utilizing multiple images. Schaul et al. proposed to fuse the near infrared (NIR) image into the visible image[2]. This method can recover details and texture even if the visible image loses them. However, the result images look unnatural because NIR images have some different properties from visible images.

In this paper, we propose a novel dehazing method to fuse the visible and the NIR images of the same scene. By weighting the NIR image with the transmission map, our approach fuses the NIR and the visible images in the haze regions. Therefore, our method can create a natural and clear images.

(a) (b)

Figure 1: Examples of visible and NIR images. (a) visible image. (b)NIR image.

2. RELATED WORK

2.1. NIR IMAGE

Wavelength of the visible band is 400-700 nm while that of the NIR band is 700-1100 nm. Thus NIR images have some features different from visible images[3]. Fig.1 shows visible and NIR images.

First, NIR images have less influence of Rayleigh scattering. It is the scattering phenomenon of light when atmospheric particles are smaller than the wavelength of light. This phenomenon is related to occurrence of haze. Rayleigh scattering can be expressed as

$$E_s \propto \frac{E_0}{\lambda^4}, \tag{1}$$

where E_s is the intensity of the scattered light, E_0 is the incident light, λ is the wavelength. In Eq.1, NIR images are less scattered than visible images because the NIR wavelength are longer. Therefore, haze is much less present.

Secondly, vegetation is captured with high luminance in NIR image because of the chlorophyll.

2.2. TRASMISSION MAP

In this section, we introduce the way to obtain the transmission map. The transmission map shows the portion of the light that is not scattered and reaches to the camera. We use He's method[1] to obtain the transmission map.

In general, the haze image model widely used to explain the structure of the haze image is[1]:

$$\mathbf{I}(\mathbf{x}) = \mathbf{J}(\mathbf{x})t(\mathbf{x}) + \mathbf{A}(1 - t(\mathbf{x})) \tag{2}$$

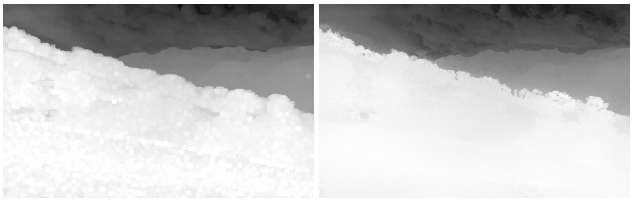

(a) (b)

Figure 2: Transmission maps. (a) Original transmission map. (b) Refined transmission map.

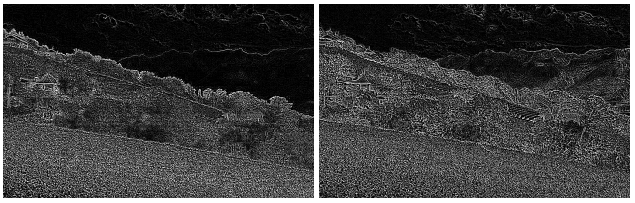

(a) (b)

Figure 3: Laplacian images. (a)Laplacian image of luminance image . (b) Laplacian image of NIR image.

where **I** is the observed image, **J** is the haze-free image, **A** is the atmospheric light, t is the transmission, and **x** is a pixel index. To obtain the transmission map, we estimate the transmission using Eq.2.

To estimate the transmission, we apply dark channel prior Eq.2. Moreover, we assume that the transmission t in a local patch is constant:

$$\begin{aligned}\min_{\mathbf{y}\in\Omega(\mathbf{x})}\left(\min_{c\in\{r,g,b\}}\frac{I^c(\mathbf{y})}{A^c}\right)\\ =\tilde{t}(\mathbf{x})\min_{\mathbf{y}\in\Omega(\mathbf{x})}\left(\min_{c\in\{r,g,b\}}\frac{J^c(\mathbf{y})}{A^c}\right)+1-\tilde{t}(\mathbf{x})\end{aligned} \tag{3}$$

where Ω is the local patch and c is the color channel. $\tilde{t}$ shows the transmission t is constant. Thus, it can be taken out of the min operators.

Since **J** is the haze-free image, the dark channel of J is nearly zero. Therefore, we can estimate the transmission $\tilde{t}$ simply by

$$\tilde{t}(\mathbf{x})=1-\min_{\mathbf{y}\in\Omega(\mathbf{x})}\left(\min_{c\in\{r,g,b\}}\frac{I^c(\mathbf{y})}{A^c}\right) \tag{4}$$

However, people perceive depth by the presence of haze. If we remove the haze completely, the image may be unnatural. So we need to leave a very little haze for the distant objects. We add a constant parameter ω into Eq.4:

$$\tilde{t}(\mathbf{x})=1-\omega\min_{\mathbf{y}\in\Omega(\mathbf{x})}\left(\min_{c\in\{r,g,b\}}\frac{I^c(\mathbf{y})}{A^c}\right) \tag{5}$$

In this paper, the value of ω is 0.95. We can obtain the transmission map using Eq.5. Fig.2(a) shows the obtained transmission map. It can be seen that there are block artifacts. This is because we set the local patch to calculate the dark channel. To eliminate block artifacts, we use the guided filter[4]. Fig.2(b) shows refined transmission map. we use the color input image as a guide.

3. DEHAZING METHOD

In our dehazing method, we first the luminance image and the transmission map from the visible image. We use the luminance image because NIR images have only luminance information. Next, we decompose the luminance image, the transmission map, and the NIR image using Laplacian pyramid, and the Laplacian images of the NIR image are weighted with the transmission map. Then Laplacian images of the luminance image and NIR image is compared and fused. The new luminance image is reconstructed based on the fused Laplacian image. Finally, the result image is obtained by recombining the new luminance image and the chrominance information of the visible image.

3.1. LAPALACIAN PYRAMID

Laplacian pyramid[5] is one of multi-resolution analysis methods. It is simple and fast; therefore we use this method.

We transform the luminance image V, the NIR image N, the transmission map t into multi-resolution representation using Laplacian pyramid. First, we obtain Gaussian pyramid G_k, it is defined by

$$G_k=[f*G_{k-1}]_{\downarrow 2}\quad(k=1,2,\cdots) \tag{6}$$

Where f is the Gaussian filter, k is the number of level and G_0 is equal to V.

Secondly, we obtain the Laplacian pyramid. The Laplacian pyramid L_k is defined by

$$L_k=G_k-4w*[G_{k+1}]_{\uparrow 2}\quad(k=0,1,\cdots) \tag{7}$$

the images are decomposed using this method. Laplacian images of V and N is shown in Fig.3. We can see that details appear more the Laplacian image of V than that of N.

3.2. WEIGHTING THE NIR IMAGE

We need to put NIR information into the luminance image V in the only haze region because NIR images have some different features from visible images. If NIR information is fused to V in the haze-free region, the result image will be unnatural. Therefore, we weight the Laplacian image of the NIR image N_k^l with the Gaussian image of the transmission

(a) (b) (c) (d)

Figure 4: (a) A haze image and the dehazed image using (b) 3, (c) 5, and (d) 7 pyramid levels, respectively.

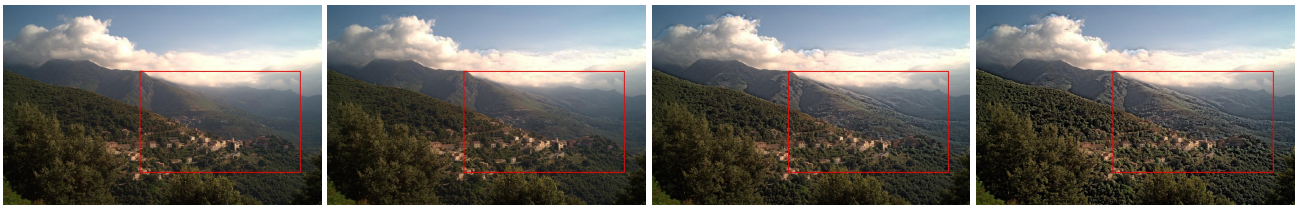

(a) (b) (c) (d)

Figure 5: (a) A haze image and the dehazed image using (b) 50, (c) 150, and (d) 250 parameters a, respectively.

(a) (b) (c) (d)

Figure 6: Expanded images in the red rectangle in Fig.5. (a)Haze image. (b) 50, (c) 150, (d) 250 parameters a, respectively.

map t_k^g:

$$\tilde{N_k^l}(\mathbf{x}) = \begin{cases} N_k^l(\mathbf{x}) \times \frac{a}{t(\mathbf{x})_k^g} & (a < t(\mathbf{x})_k^g) \\ N_k^l(\mathbf{x}) & (t(\mathbf{x})_k^g \leq a) \end{cases} \quad (8)$$

$\tilde{N_k^l}$ is weighted Laplacian image of NIR image. We optionally set a parameter a as a criterion haze exist in transmission map. when the value of transmission map is lager than the parameter a, N_k^l is weighted. As a result, NIR image isn't fused in the haze-free region. Eq.8 can perform that we put the NIR information into V in the only haze region.

3.3. COMPARISON AND FUSING

To fuse the Laplacian image of the luminance image V and the NIR image $\tilde{N^l}$, we compare them. First, we consider a local patch centered at a pixel to compare, and we calculate the square of pixel values in the local patch. We compare the images by the sum:

$$\tilde{L_k}(\mathbf{x}) = \begin{cases} V_k^l(\mathbf{x}) & (V_s(\mathbf{x}) > N_s(\mathbf{x})) \\ \tilde{N_k^l}(\mathbf{x}) & (\text{ohterwise}) \end{cases} \quad (9)$$

where $\tilde{L_k}$ is the new Laplacian image, V_k^l is the Laplacian image of V, V_s is the sum of the $(V_k^l)^2$, and N_s is the sum of $(\tilde{N_k^l})^2$ in the local patch. They are calculated using the local patch size 3×3. The Laplacian image of the maximum of the V_s and the N_s is selected by Eq.9. The final fused image is reconstructed using the new Laplacian images.

4. EXPERIMENTAL RESULTS

Fig.4 shows the dehazed results using different pyramid levels. The image sizes are 1024×640. As the pyramid level rises, the result images appear unnatural. In this paper, we use a pyramid level of 3.

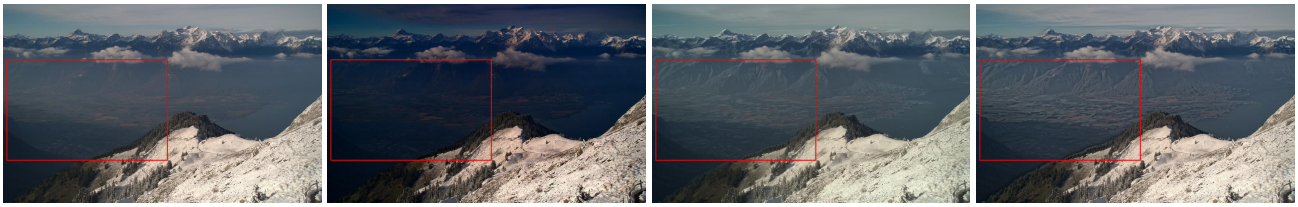

(a) (b) (c) (d)

Figure 7: Comparison with other methods. (a)Haze image. (b) He et al.'s result [1]. (c) schaul et al.'s result [2]. (d) Our result.

(a) (b) (c) (d)

Figure 8: Expanded images in the red rectangle in Fig.7. (a)Haze image. (b) He et al.'s result [1]. (c) schaul et al.'s result [2]. (d) Our result.

Fig.5 shows the dehazed images using different parameter a. And furthermore, Fig.6 shows expanded images in the red rectangle in Fig.5. In Fig.6(b), the parameter a is 50. the result image almost leave haze. In Figs.6(c) and 6(d), the parameters a are 150 and 250, respectively. The result images can reduce haze and recover the details. However, in Fig.6(d), the haze-free region was unnatural. This is because the NIR image is fused in the haze-free region owing to the parameter a was high. Therefore, we use the parameter a of 150.

In Fig.7, we compare our method with other methods. We can see that our result recovers the original color of the scene than the other methods. Fig.8 shows the expanded images in the red rectangle in Fig.7. He et al.'s result can't recover details and texture because the method uses only the visible image. Compared with Schaul et al.'s result, our result can see them clearly.

5. CONCLUSION

In this paper, we have proposed a novel dehazing method. Our approach is based on fusing visible and NIR images. Weighting the NIR image with a transmission map, we can put the NIR information into the visible image in the only haze region. Color image dehazing becomes more effective. However, we can see that our result don't completely remove haze. As NIR images are gray scale images, our method doesn't deal with color information. We consider that result images is improved using color information. In the future, we want to investigate a method to obtain more clear image.

REFERENCES

[1] K. He, J. Sun and X. Tang, "Single Image Haze Removal Using Dark Channel Prior," IEEE Transactions on Pattern Analysis and Machine Intelligence, vol. 33, no. 12, pp. 2341–2353, Dec. 2011.

[2] L. Schaul, C. Fredembach and S. Süsstrunk, "Color Image Dehazing Using the Near-Infrared," Proc. IEEE International Conference on Image Processing, pp. 1–4, Nov. 2009.

[3] C. Fredembach and S. Süsstrunk, "Colouring the Near-Infrared," IS&T 16th Color Imaging Conference, pp. 176–182, 2008.

[4] K. He, J. Sun and X. Tang, "Guided Image Filtering," IEEE Transactions on Pattern Analysis and Machine Intelligence, vol. 35, no. 6, pp. 1397–1409 Jun. 2013.

[5] P. J. Burt, R. J. Kolczynski, "Enhanced Image Capture Through Fusion," Proc. Fourth International Conference on Computer Vision , pp. 173–182, May. 1993.